Biochimica et Biophysica Acta 1848 (2015) 878–885

Contents lists available at ScienceDirect

Biochimica et Biophysica Acta

journal homepage: www.elsevier.com/locate/bbamem

Structure of the N-terminal segment of human retinol dehydrogenase 11 and its preferential lipid binding using model membranes

Mustapha Lhor, Mario Méthot, Habib Horchani, Christian Salesse *

CUO–Recherche, Hôpital du Saint-Sacrement, Centre de recherche du CHU de Québec and Département d'ophtalmologie, Faculté de médecine, and Regroupement stratégique PROTEO, Université Laval, Québec, Québec, Canada

ARTICLE INFO

Article history:
Received 5 October 2014
Received in revised form 9 December 2014
Accepted 15 December 2014
Available online 24 December 2014

Keywords:
Retinol dehydrogenase 11
N-terminal anchoring peptide, monolayer
Protein secondary structure
Maximum insertion pressure
Retinal pigment epithelium

ABSTRACT

Retinol dehydrogenase 11 (RDH11) has been postulated to be anchored to membranes by means of its N-terminal segment in retinal pigment epithelial (RPE) cells where it participates to the visual cycle. The analysis of the primary sequence of RDH11 revealed that its N-terminal hydrophobic segment could be involved in the anchoring of this enzyme to membranes. However, no information is yet available on the properties of this N-terminal segment to support this role. The secondary structure and membrane binding of two N-terminal peptides of RDH11 with different lengths have thus been investigated to provide this information. Online tools allowed predicting an α-helical secondary structure for both peptides. Infrared spectroscopy and circular dichroism have shown that the α-helix of the Long-peptide (35 amino acids) is longer and more rigid than that of the Short-peptide (25 amino acids) regardless of the type of solvent. Langmuir monolayers have been used as a model membrane to study lipid–peptide interactions. Values of maximum insertion pressure and synergy suggested a preferential binding of the Long-peptide to lipids with a phosphoethanolamine polar head group, which are abundant in the RPE. Furthermore, infrared spectroscopy in monolayers has shown that the α-helical structure of the Long-peptide is more stable in the presence of saturated phospholipids whereas the structure of the Short-peptide is mainly disordered. Altogether, the present data demonstrate that the α-helical hydrophobic core of the N-terminal segment of RDH11 displays properties typical of transmembrane domains, in agreement with its postulated role in the membrane anchoring of this protein.

1. Introduction

Human retinol dehydrogenase 11 (EC1.1.1.315) (RDH11) is a 318 amino acid (~35 kDa) enzyme belonging to the short-chain dehydrogenases/reductases (SDR) family. It is found in different tissues such as brain, testis and prostate where it was initially designated as PSDR1 [1]. It was also named RalR1 in reference to its retinal reductase activity [2]. During the retinoid visual cycle, this enzyme is partly responsible for the conversion of 11-*cis* retinol into 11-*cis* retinal in the retinal pigment epithelium (RPE) [2,3], whereas most of this activity is assumed by RDH5 [4]. Like other RDHs, its catalytic activity has been characterized *in vitro* [5]. It was shown that RDH11 can use both *cis* and *trans* substrates, with NADP(H) as the preferred cofactor [2]. However, RDH11 has no steroid activity in contrast to other SDRs [6].

Several data suggest that RDH11 is associated with membranes [7]. Indeed, it has been shown that the residual 11-*cis* RDH activity in the $RDH5^{-/-}$ mice, assigned to RDH11, is membrane-associated [8] which was consistent with the subcellular location of this enzyme [7]. In addition, a hydropathy analysis of the primary sequence of RDH11 revealed the presence of a hydrophobic segment in its N-terminal region (amino acids 2 to 22) [7]. The putative membrane-anchoring role of this segment was studied with recombinant RDH11 produced in insect sf9 cells; the enzyme was shown to target microsomal membranes. The analysis of the amino acid sequence of this N-terminal segment allowed postulating that the arginine/lysine motif flanking this segment mediates membrane-anchoring of RDH11 and prevents its translocation across the membrane [7]. Nevertheless, structural information and membrane binding characteristics of the N-terminal anchoring segment of RDH11 are still lacking.

The aim of the present study was thus to gather information on the secondary structure of the putative anchoring segment of RDH11 and its preferential binding features toward phospholipids. In order to get

Abbreviations: ATR, attenuated total reflectance; CD, circular dichroism; DOPE, 1,2 dioleoyl-sn-glycero-3-phosphoethanolamine; DOPC, 1,2-dioleoyl-sn-glycero-3-phosphocholine; DOPS, 1,2-dioleoyl-sn-glycero-3-phosphoserine; DPPE, 1,2-dipalmitoyl-sn-glycero-3-phosphoethanolamine; DSPE, 1,2-distearoyl-sn-glycero-3-phosphoethanolamine; DDPE, 1,2-didocosahexaenoyl-sn-glycero-3-phosphoethanolamine; HFIP, hexafluoroisopropanol; MeOH, methanol; MIP, maximum insertion pressure; PM-IRRAS, polarization modulation infrared reflection absorption spectroscopy; RDH11, retinol dehydrogenase 11; RPE, retinal pigment epithelium; SDR, short-chain dehydrogenase reductase; TM, transmembrane

* Corresponding author at: CUO–Recherche, Centre de recherche du CHU de Québec, Hôpital du Saint-Sacrement, 1050 Chemin Ste-Foy Québec, Québec, Canada G1S 4L8. Tel.: +1 418 682 7569; fax: +1 418 682 8000.
E-mail address: christian.salesse@fmed.ulaval.ca (C. Salesse).

http://dx.doi.org/10.1016/j.bbamem.2014.12.014
0005-2736/

insights on the particular region required to confer membrane anchoring of RDH11, two peptides with different lengths have been studied because typical transmembrane segments vary significantly from less than 15 up to 40 amino acids [9–12]. The hydrophobicity of their primary structure has thus been analyzed and their secondary structure has been predicted using the online tool I-TASSER [13,14]. The secondary structure of these peptides has then been studied using circular dichroism and infrared spectroscopy, which are commonly used to probe the secondary structures of proteins and peptides [15–17]. Furthermore, the membrane binding and secondary structure of these peptides have been investigated using Langmuir monolayers as a model membrane by performing surface pressure and infrared spectroscopic measurements, respectively [14].

2. Materials and methods

2.1. Materials

The deionized water used for the preparation of buffer solutions was highly purified with a Milli-Q water purification system from Millipore (Billerica, MA, USA). This water had a resistivity of no less than 18.2 MΩ.cm and a surface tension of 72 ± 0.1 mN/m at room temperature. All lipids used were purchased from Avanti Polar Lipids (Alabaster, AL, USA): 1,2-dioleoyl-sn-glycero-3-phosphoethanolamine (DOPE), 1,2-dioleoyl-sn-glycero-3-phosphocholine (DOPC), 1,2-dioleoyl-sn-glycero-3-phosphoserine (DOPS), 1,2-dipalmitoyl-sn-glycero-3-phosphoethanolamine (DPPE), 1,2-distearoyl-sn-glycero-3-phosphoethanolamine (DSPE), 1,2-didocosahexaenoyl-sn-glycero-3-phosphoethanolamine (DDPE). These phospholipids were solubilized in chloroform: methanol (9:1, v:v) to get a final concentration of 0.2 mg/ml. To prevent oxidation, BHT was added to the unsaturated phospholipids at a final molar ratio of 1:200 (mole of BHT: mole of phospholipids) and they were sealed under argon. BHT has been previously shown to have no effect on the isotherm of phospholipids [18]. Chloroform, hexafluoroisopropanol (HFIP), methanol (MeOH) and Tris-HCl were from Laboratoire MAT (Québec, Canada). NaCl and β-mercaptoethanol were from Sigma (St. Louis, MO, USA). All chemicals were used as received. The Long- (VELMFPLLLLLLPFLLYMAAPQIRKM LSSGVCTST, purity >93%; molecular mass: 3910.9 g/mol) and Short- (VELMFPLLLLLLPFLYMAAPQIRK, purity >95%; molecular mass: 2943.8 g/mol) peptides corresponding to different lengths of the N-terminal segment of RDH11 were synthesized by Peptides 2.0 (Chantilly, VA, USA). The identity and purity of these peptides were confirmed by a combined HPLC-MS analysis. Peptides were solubilized in hexafluoroisopropanol or in methanol.

2.2. Methods

2.2.1. Hydrophobicity pattern and structural model of the Long- and Short-peptides

The hydrophobicity of the N-terminal peptides of RDH11 has been evaluated using the Heliquest online program [19] and values of mean hydrophobicity <H> and mean hydrophobic moment <μH> were used to produce the associated Eisenberg plot [20]. In addition, the 35 and 25 amino acids sequence corresponding, respectively, to the Long- and Short-peptides of the N-terminal segment of RDH11 were uploaded on the online server (http://heliquest.ipmc.cnrs.fr) to predict their structure with the helical wheel module using a full length window analysis. Moreover, a 3D-model of the structure of these peptides was predicted with the I-TASSER server [13,21]. This algorithm allowed creating five *ab initio* structures. The selected 3D structure was the one showing the highest confidence score (C-score).

2.2.2. Circular dichroism analyses of the Long- and Short-peptides

Circular dichroic spectra were recorded with a Jasco spectropolarimeter (Model J-815, Jasco, Easton, MD, USA) at room temperature. The spectra have been measured at a peptide concentration of 150 μM in HFIP and MeOH. For each spectrum, 10 scans were collected in the far-UV range from 190 to 260 nm, using a 1 mm path length cuvette. The solvent contribution was subtracted from the spectrum of the peptide. The peptide concentration in mol/L has been calculated as follows: protein concentration (g/L) x number of amino acids/molar mass. The different spectra can thus be properly compared because the molar ellipticity takes into account the number of amino acids of each individual peptide.

2.2.3. Infrared spectroscopy of the Long- and Short-peptides

Infrared spectra were recorded using a Nicolet Magna 850 FTIR spectrometer (Thermo Scientific, Madison, WI, USA) equipped with a liquid nitrogen cooled narrow-band mercury cadmium telluride detector and a Golden Gate attenuated total reflection (ATR) accessory. A drop of 50 μl of the Short- or Long-peptides (at a concentration of 150 μM) was deposited on the stage of the Golden Gate and the spectrum was measured. The spectrum of the pure peptide was obtained by subtracting that of the solvent. An infrared spectrum of the peptide powder was also measured using the same setting. The maximum of amide I band has been determined by performing the analysis of the second derivative or by Fourier deconvolution of the spectra. All spectra were treated using the Omnic software available with the spectrometer.

2.2.4. Determination of the maximum insertion pressure and synergy of the Long- and Short-peptides upon monolayer binding

Measurement of the binding of the Short- and Long-peptides onto different lipid monolayers was performed using a Kibron DeltaPi-4 microtensiometer and a multiwell glass plate (Kibron Inc., Helsinki, Finland). The optimal peptide concentration to reach surface saturation has been determined by performing measurements of the increase in surface pressure at different peptide concentrations in the absence of a phospholipid monolayer. The surface saturation for the Short- and Long-peptides has been reached at a concentration of 1.25 μM (data not shown). Phospholipids were slowly spread using a Hamilton microsyringe (Reno, NV, USA) at the surface of the monolayer buffer (50 mM Tris HCl, 150 mM NaCl and 5 mM β-mercaptoethanol (pH 7.4)) poured in a 500 μL trough of the multiwell glass plate until the desired surface pressure was reached. The waiting time period for the spreading solvent evaporation and for the film to reach equilibrium varied with the type of lipid, the spreading volume, the initial surface pressure, and the lipid concentration [22]. Then, 5 μL of peptide in MeOH was injected into the subphase underneath the phospholipid monolayer to reach a final concentration of 1.25 μM. Methanolic solutions of the peptides were used because this solvent is highly miscible with water and does not perturb the surface pressure measurements. Measurements were performed at different initial surface pressures (Πi) until the equilibrium surface pressure (Πe) was reached. This allowed calculation of the surface pressure increase (ΔΠ) using $\Delta\Pi = \Pi e - \Pi i$. The plot of ΔΠ as a function of Πi allowed determining the MIP (maximum insertion pressure) by extrapolating the regression of the curve to the x-axis [22]. The values of MIP can be used to compare the extent of peptide binding onto lipid monolayers [18,22–24]. Synergy is calculated by adding 1 to the slope of the plot of ΔΠ as a function of Πi [18]. The calculation of the uncertainty of the values of MIP and synergy were performed as previously described [22] and by using a dedicated online tool: http://www.crchudequebec.ulaval.ca/BindingParametersCalculator.

2.2.5. Monitoring of the secondary structure of the Long- and Short-peptides in monolayers by infrared spectroscopy

Polarization modulation infrared reflexion absorption spectroscopy (PM-IRRAS) was performed as described previously [25–28]. Briefly, PM-IRRAS combines Fourier transform mid-IR reflection spectroscopy

(FT-IR) with rapid polarization modulation of the incident beam [29,30]. To remove the isotropic contributions from bulk water and water vapor as well as experimental drifts and to get rid of the dependence on the Bessel function, the spectrum of the peptide in the presence or in the absence of the phospholipid monolayer was respectively divided by that of the lipid or of the buffer to produce the resulting normalized PM-IRRAS spectrum. Each PM-IRRAS spectrum was the result of the coaddition of 800 scans at a resolution of 8 cm^{-1}. In these experiments, the monolayer buffer (see Section 2.2.4) was poured in a 8 mL Teflon trough. Phospholipids were then slowly spread at the surface of the buffer until the desired surface pressure was reached (~10 mN/m). After a waiting period of ~30 min, 80 μL of the peptide in methanol was injected into the subphase to reach a final concentration of 1.25 μM. Surface pressure was monitored with a NIMA tensiometer (Coventry, UK) during the measurement of the infrared spectra at an equilibrium surface pressure of ~20-25 mN/m depending on the initial surface pressure and the type of phospholipid.

3. Results

3.1. Analysis of the primary sequence of the Long- and Short-peptides

The amino acid sequence of the Long- and Short-peptides is presented in Table 1. The initial methionine produced by the starting codon does not appear in these sequences because it is normally cleaved *in vivo* by the N-terminal methionine excision machinery [31,32]. The larger values of mean hydrophobic moment <μH> and mean hydrophobicity <H> for the Short-peptide suggest that it is more hydrophobic than the Long-peptide (Table 1). Moreover, the projection of their amino acid sequence in the helical wheel representation (Supplementary Figure S1A and B) strongly suggests that they are not amphipathic peptides. In fact, it can be seen that the Short-peptide contains a larger proportion of hydrophobic amino acids (21/25, 84%; Table 1 and Supplementary Figure S1B) than the Long-peptide (24/35, 69%; Table 1 and Supplementary Figure S1A). However, it can be seen that both peptides include an extremely hydrophobic core from amino acids Val2 to Pro22, on the basis of the analysis reported on the Uniprot website (accession #Q8TC12) as well as that performed using the Heliquest server (Supplementary Figure S1C). Moreover, as shown in Table 1 and Supplementary Figure S1A, the presence of a glycine and several additional polar amino acids, such as serine, threonine and glutamine, likely increases the hydrophilic character of the Long-peptide compared to the short one, which is consistent with the hydrophobicity values. The highly hydrophobic core (Val2–Pro22) likely corresponds to the segment of the peptide located within the hydrophobic layer of the membrane. Our prediction model of this hydrophobic core as an α-helical structure (see inset of Fig. 2) allowed us to estimate its length to ~26 Å using PyMOL which fits well with that of the membrane hydrophobic layer lying in the range of 20-30 Å [33,34]. Moreover, the values of the hydrophobic moment <μH> and the mean hydrophobicity <H> allowed locating these peptides in the transmembrane region on the Eisenberg plot (Fig. 1). In fact, peptides

Table 1
Primary structure and hydrophobicity pattern of the Long- and Short-peptides. The position and the amino acid sequence of the peptides refer to the N-terminal segment of human RDH11. <H> and <μH> respectively correspond to the mean hydrophobicity and the mean hydrophobic moment. They were obtained using the Heliquest online server. Underlined amino acids correspond to the potential transmembrane domain of RDH11. They have been identified on the Uniprot website (V_2-P_{22}; accession #Q8TC12).

Peptide	Position	Sequence	<H>	<μH>
Long	2-36	**VELMFPLLLLLLPFLLYMAAPQIRKMLSSGVCTST**	0.89	0.09
Short	2-26	**VELMFPLLLLLLPFLLYMAAPQIRK**	1.01	0.16

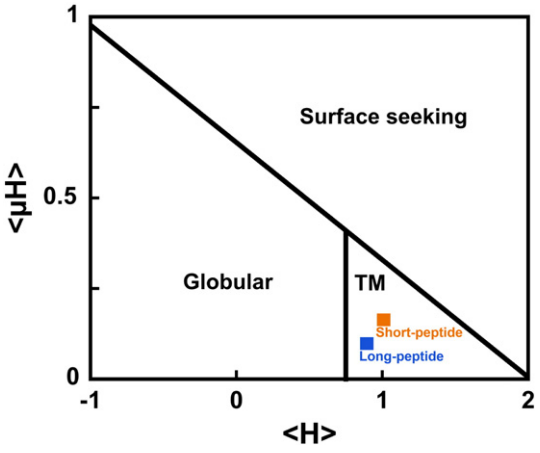

Fig. 1. Eisenberg plot of the RDH11 peptides obtained form the Heliquest generated data. The Long- and Short-peptides are located in the transmembrane region (TM).

are generally considered as potential transmembrane segments when their mean hydrophobicity <H> (Table 1) is larger than 0.75 [20].

3.2. Determination of the secondary structure of the Long- and Short-peptides in solution

3.2.1. Circular dichroism analyses of the Long- and Short-peptides

Fig. 2 presents the circular dichroism spectra of the Short- and Long-peptides. All spectra are showing a shape that is typical of α-helices [35]. Indeed, the characteristic negative bands of α-helices can be observed at ~208 and ~222 nm as well as a positive band at ~195 nm. Given that the molar ellipticity takes into account the number of amino acids of each individual peptide, the larger ellipticity of the Long-peptide (Fig. 2) demonstrates that its α-helix is better structured than that of the Short-peptide. The predicted secondary structure of the Long- and Short-peptides using the I-TASSER server are schematically presented in the inset of Fig. 2. The α-helical prediction of these peptides is in good agreement with the observation of dichroic spectra that are typical of α-helices. In addition, a shift of the spectra of the peptides in HFIP to lower wavelengths can also be observed, which suggests a smaller α-helical content in this solvent. This observation was

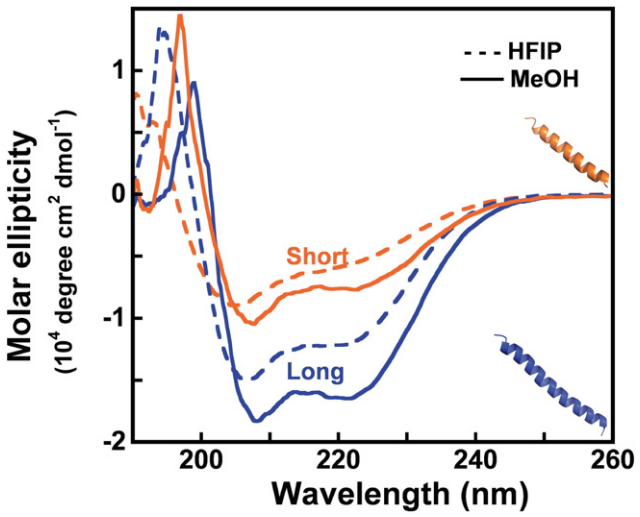

Fig. 2. Circular dichroic spectra of the Long- and Short-peptides in different solvents: HFIP (dashed line) and MeOH (solid line). Inset: 3D structural model of RDH11 peptides obtained using I-TASSER (the α-helical structural model of the Long- and Short-peptides is the same color as that of the corresponding experimental curves).

surprising in view of the known enhancing effect of this solvent on the content of α-helices [36,37]. It has been shown that circular dichroism is accurate for α-helical structure predictions whereas infrared spectroscopy performs better for β-sheet estimation [38]. Infrared spectroscopy has thus been used to get additional information of the secondary structure of these peptides.

3.2.2. Infrared spectroscopy analyses of the Long- and Short-peptides

Infrared spectroscopy is well known to allow evaluating the secondary structure of peptides and proteins [17,39]. The amide I absorption band between 1400 and 1800 cm^{-1} is associated mainly to the C = O stretching vibration as well as minor contributions from the out-of-phase C-N stretching vibration of the peptide bonds, which allow to get secondary structure backbone information [17]. Fig. 3 presents the infrared spectra of the Long- and Short-peptides in solution as well as in powder. A variety of solvents were tested to solubilize peptides but methanol and HFIP were the most appropriate ones. As shown in Fig. 3A, the Long-peptide presents a characteristic spectrum of α-helices with a symmetrical amide I band centered at 1653 and 1658 cm^{-1} when it is solubilized in HFIP and MeOH, respectively. It has been shown that a maximum close to 1650 cm^{-1} indicates a long and rigid α-helical structure. This position can shift up to 1662 cm^{-1} when the α-helix progressively unwinds [40,41]. This takes place, in particular, in polar solvents such as water and methanol where the end of the α-helix transiently unwinds as a result of hydrogen bonding between the amide groups and the polar solvent. This phenomenon is less favorable in hydrophobic solvents because they have much less affinity for the polar amide groups. The shift from 1653 in HFIP (hydrophobic solvent) to 1658 cm^{-1} in methanol (polar solvent) can thus be explained by a partial unwinding of the end of the α-helix of the Long-peptide in methanol. This observation of longer and more rigid α-helices in HFIP is consistent with its well known effect in enhancing α-helical structures [36,37] but this is inconsistent with the decrease in ellipticity observed by circular dichroism in this solvent (Fig. 2, Section 3.2.1). The predicted secondary structure (inset of Fig. 2) is in good agreement with the helical content of the Long-peptide as well as its high hydrophobicity (Table 1 and Supplementary Figure S1A). Moreover, a long and rigid α-helical structure also exists in the Long-peptide powder since a large spectral overlap is observed between its amide I band and that in HFIP (Fig. 3A). The amide I band of the Short-peptide in MeOH is centered at 1658 cm^{-1} whereas that in HFIP is slightly wider and shifted to 1653 cm^{-1} (Fig. 3B). These data suggest that this peptide also folds as an α-helix in these solvents although it probably includes additional secondary structure components when solubilized in HFIP on the basis of its larger amide I band width. In contrast, the amide I band of the Short-peptide powder is much wider than those in MeOH and HFIP and thus likely contains random coil or disordered structures (1642-1654 cm^{-1}) or aggregated β-sheets (1620-1625 cm^{-1}) in addition to α-helices (for a review, see [17]). Taken together, these findings suggest that the Long-peptide forms a longer and more rigid α-helix than that of the Short-peptide, in particular in HFIP.

3.3. Binding of the Long- and Short-peptides to different lipid monolayers

Lipid monolayers are very useful model membranes to determine the extent of binding of peptides and proteins [14,42,43]. Values of MIP of peptides and proteins in the presence of different phospholipids provide information on their affinity for particular lipids [18,22]. To perform these measurements, we have selected lipids that can be found in the membranes where RDH11 is located. The phospholipid content of RPE membranes in the macula or in the periphery is quite similar. It includes 67% phosphoethanolamine (PE), 20% phosphocholine (PC), 9% phosphoinositol (PI) and 4% phosphoserine (PS) [44]. In addition, the major fatty acyl chains found in phospholipids of the RPE are palmitoyl (C16:0), stearoyl (C18:0), oleoyl (C18:1ω9) and docosahexaenoyl (C22:6ω3) [44]. Given that phospholipids bearing oleoyl fatty acyl chains are the most abundant ones in the RPE and that the phospholipid found in largest amount is phosphoethanolamine, phospholipids bearing palmitoyl (DPPE), stearoyl (DSPE), oleoyl (DOPE, DOPC and DOPS) and docosahexaenoyl (DDPE) fatty acyl chains have thus been selected to perform measurements of the monolayer binding of the N-terminal peptides of RDH11. As presented in Fig. 4A, similar values of MIP have been obtained for the Short- and the Long-peptides when individual phospholipids are compared. Moreover, the values of MIP obtained with all phospholipids are larger than the estimated membrane lateral pressure of 30–35 mN/m [45], thus suggesting that both peptides can bind membranes of RPE cells. It is interesting to first compare the MIP values obtained when using phospholipids with the same fatty acyl chain but with different polar head groups. MIP values of 44.4 ± 3.4, 37.8 ± 2.3 and 35.7 ± 2.3 mN/m have thus respectively been obtained for the Long-peptide in the presence of DOPE, DOPC and DOPS (Fig. 3A). Given that there is no significant difference between the MIP of the Long- and Short-peptides in the presence of the zwitterionic DOPC and the negatively charged DOPS, it can be postulated that the net positive charge of these peptides is not involved in this binding process. Similar values have been obtained for the Short-peptide. These data are suggesting a slight preference of both peptides for DOPE. Measurements were then performed with phosphoethanolamine bearing different fatty acyl chains (16:0, 18:0 and 22:6) to assess the effect of the physical state and polyunsaturation on peptide binding. Values of MIP of 37.9 ± 2.4, 47.5 ± 3.1 and 41.9 ± 2.7 mN/m

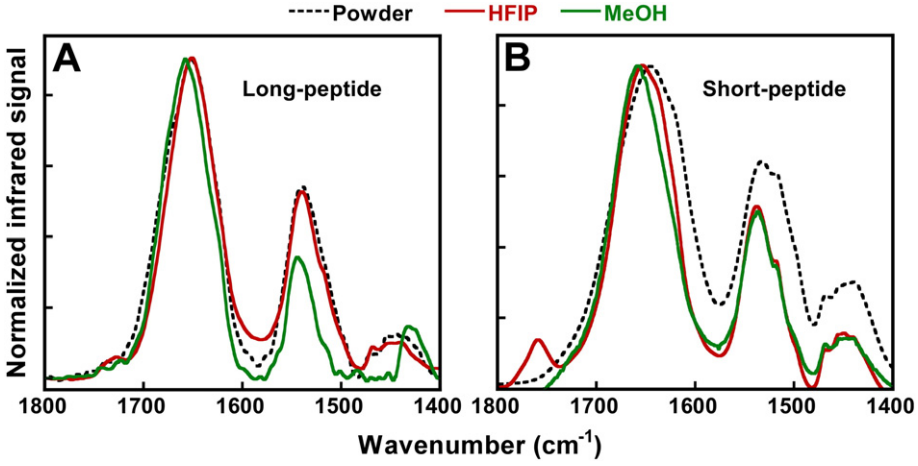

Fig. 3. Infrared spectra of the Long- **(A)** and Short-peptides **(B)**. For each peptide, spectra were measured as powder (black dashed line) or in solution (HFIP, red; MeOH, green). Spectra have been normalized to facilitate their comparison.

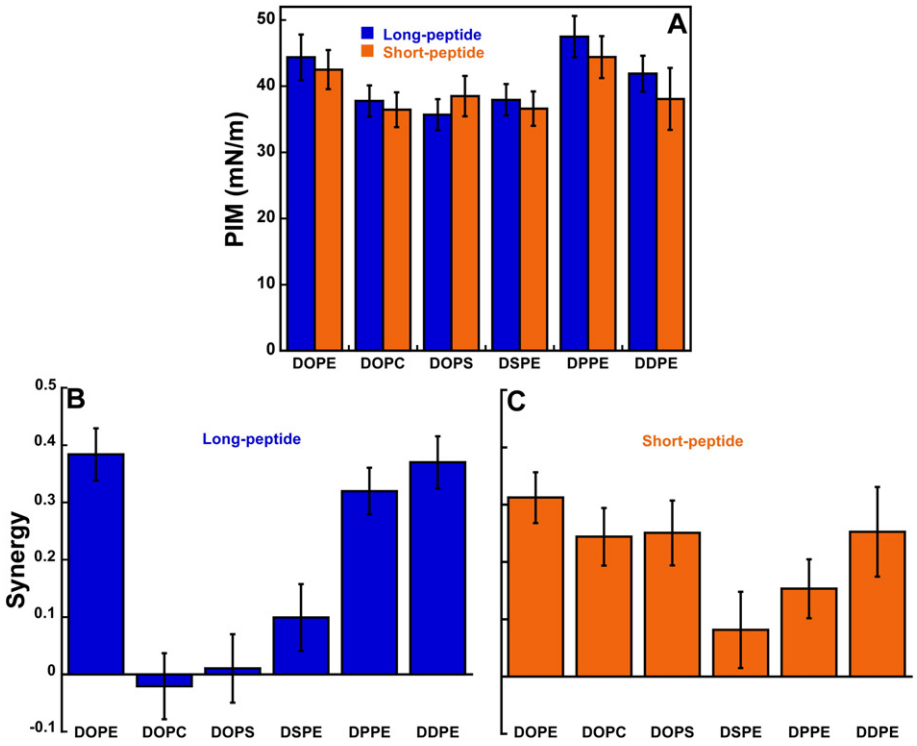

Fig. 4. Maximum insertion pressure (MIP) of the Long- and Short-peptides obtained in presence of different unsaturated (DOPE, DOPC, DOPS, DDPE) and saturated (DPPE, DSPE) phospholipid monolayers **(A)**. Synergy values of the Long- **(B)** and Short-peptides **(C)** were determined in presence of the same phospholipids. Peptides are injected into the monolayer subphase containing 50 mM Tris HCl, pH 7.4, 150 mM NaCl and 5 mM β-mercaptoethanol. The final concentration of the peptides in the subphase is 1.25 μM.

have been obtained for the Long-peptide in the presence of DSPE, DPPE and DDPE, respectively (Fig. 4A). Similar values have been obtained for the Short-peptide. A slight preference of both peptides can be observed for DPPE.

It has been established that the synergy is an additional useful binding parameter of proteins. For example, we have previously shown that the determination of synergy allowed to highlight the particular affinity of *Retinis pigmentosa* 2 for saturated phospholipids and recoverin for polyunsaturated phospholipids [18]. In the present study, synergy values of 0.38 ± 0.04, −0.02 ± 0.06, 0.01 ± 0.06, 0.1 ± 0.06, 0.32 ± 0.04 and 0.37 ± 0.04 have been obtained with the Long-peptide in the presence of DOPE, DOPC, DOPS, DSPE, DPPE and DDPE, respectively (Fig. 4B). We have previously shown that a positive synergy reveals a favorable binding whereas values of synergy close to zero suggest that there is neither attraction nor repulsion between the peptide and the monolayer [18,22]. Therefore, phosphoethanolamine highly favors binding of the Long-peptide whatever the type of fatty acyl chain, whereas DOPC and DOPS neither favor nor disfavor the binding of this peptide. The situation is quite different with the Short-peptide. Indeed, synergy values of 0.31 ± 0.04, 0.24 ± 0.05, 0.25 ± 0.06, 0.08 ± 0.06, 0.15 ± 0.05 and 0.25 ± 0.08 have been obtained for the Short-peptide in the presence of DOPE, DOPC, DOPS, DSPE, DPPE and DDPE, respectively (Fig. 4C). These data suggest that only the binding to DSPE is less favored compared to the other phospholipids.

3.4. Secondary structure of the Long- and Short-peptides upon binding to phospholipid monolayers

Infrared spectra in the amide I region can be measured using PM-IRRAS which provides information on the secondary structure of peptides and proteins in monolayers [25,26,28]. Typical spectra obtained with the Long- and Short-peptides in the absence and in the presence of different phospholipid monolayers are presented in Figs. 5 and 6. The amide I band of the Long-peptide in the absence of a phospholipid monolayer is centered at 1655 cm^{-1}, which is typical of α-helices, whereas that of the Short-peptide is shifted to 1660 cm^{-1} (Fig. 5A) and its bandwidth is much wider than that of the Long-peptide. The position and the width of the amide I band of the Short-peptide respectively suggest that its α-helix is shorter and includes more disordered structures than that of the Long-peptide. PM-IRRAS spectra of the Long-peptide in the presence of DOPE, DOPS and DOPC are shown in Fig. 5B. These spectra can be more clearly compared with that of the Long-peptide in the absence of a phospholipid monolayer in Fig. S2. It can respectively be seen in Supplementary Figures S2A, B and C that the width of the amide I band of the Long-peptide in the presence of DOPE, DOPS and DOPC is wider than that in the absence of a phospholipid monolayer. Although the shoulder observed at 1633 cm^{-1} in the amide I band of the Long-peptide/DOPE monolayer can be assigned to a β-sheet structural component, this phospholipid is the one, which least perturbs the secondary structure of this peptide when compared to DOPS and DOPC, on the basis of its smaller amide I band width. Moreover, PM-IRRAS spectra of the Long-peptide in the absence and in the presence of DPPE and DSPE are shown in Fig. 5C. The differences between these spectra and that of the Long-peptide are better appreciated in Fig. S2D (DPPE) and S2E (DSPE). A slightly larger width of the amide I band can be seen upon binding of the Long-peptide to the DPPE monolayer whereas a large overlap can be seen between the amide I band of the Long-peptide in the absence and in the presence of the DSPE monolayer. The difference between these two bands in the 1700-1800 cm^{-1} region could likely be explained by an improper subtraction of the C = O ester band of DSPE as a result of a significant perturbation of this monolayer during peptide binding (this is also likely the case for the DPPE monolayer in this range of frequency). The same spectroscopic analyses have been performed with the Short-peptide even though its secondary structure in the absence of a lipid monolayer (Fig. 5A) includes more disordered components than the Long-peptide (Fig. 6). Given that a disordered peptide can become highly structured upon monolayer binding [27], PM-IRRAS measurements were also performed with this peptide. However, as can be seen in Fig. 6A and B, the width of the amide I band of the Short-peptide is larger in the presence of DOPE,

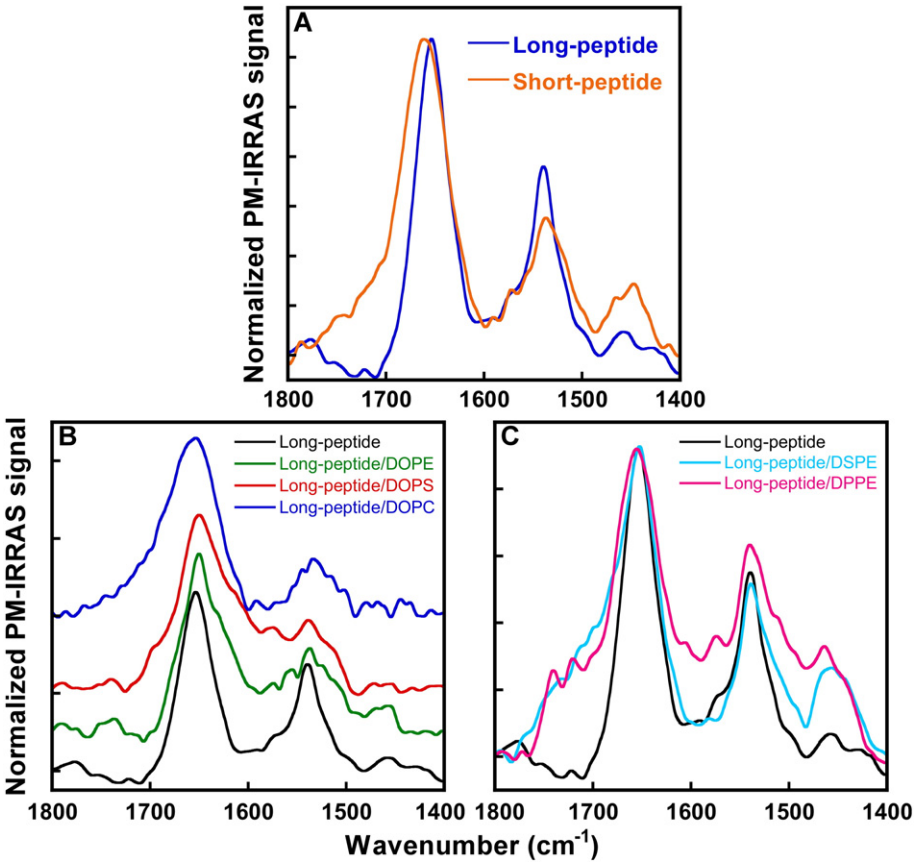

Fig. 5. PM-IRRAS spectra of the Long- and Short-peptides in the absence a phospholipid monolayer **(A)** and of the Long-peptide in the presence of a monolayer of DOPE, DOPS and DOPC **(B)**, or of DSPE and DPPE **(C)**. Spectra have been normalized to facilitate their comparison. 80 μL of peptides are injected into the monolayer subphase (see legend to Fig. 4) to reach a final concentration of 1.25 μM.

DOPS, DOPC, DPPE and DSPE than in the absence of a lipid monolayer. Therefore, none of these phospholipids allowed improving the α-helical structure of this peptide, which remained less structured than the Long-peptide upon monolayer binding.

4. Discussion

The N-terminal segment of RDH11 was postulated to allow membrane anchoring of this protein but no evidence was available to support this assertion. In this paper, the spectroscopic and monolayer binding properties of a short and a long peptide from the N-terminal segment of RDH11 have been characterized. One could have intuitively postulated that the short peptide would be more stable than the long one because of its much larger proportion in hydrophobic amino acids. The present data have however shown that this assumption was wrong, mainly from the measurements in monolayer. Indeed, we have found that the α-helical structure of the long stretch of 21 hydrophobic amino acids in the N-terminal segment of RDH11 (Table 1) are more ordered when the sequence is extended to 35 amino acids by including additional polar amino acids, such as in the Long-peptide. Therefore,

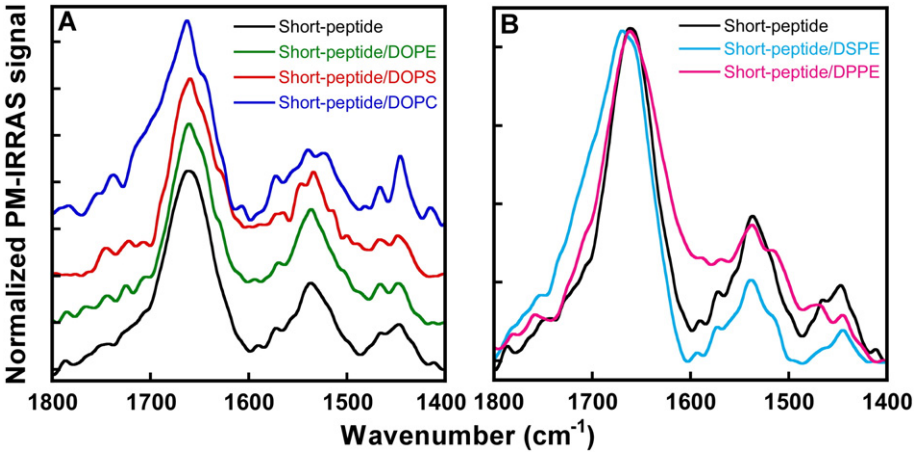

Fig. 6. PM-IRRAS spectra of the Short-peptide in the presence of a monolayer of DOPE, DOPS and DOPC **(A)** or DSPE and DPPE **(B)** (see legend to Fig. 5 for additional experimental details).

the comparison between the behavior of the 35- (Long-) and 25-amino acid (Short-) peptides of the N-terminal segment of RDH11 was found to be useful, showing that the additional polar amino acids of the Long-peptide are likely important to provide stability to the α-helical structure of the peptide. These issues are thus worth discussion.

4.1. Effect of solvents and of the adsorption of the pure Long- and Short-peptides in monolayer on their structure

Identifying an appropriate solvent to solubilize hydrophobic peptides, such as the Long- and Short-peptides of the N-terminal segment of RDH11, is a tricky and crucial task while avoiding their aggregation and/or precipitation. Such solvents should also be compatible with analytical techniques such as circular dichroism and infrared spectroscopy [46]. They should also be miscible with aqueous buffers to allow peptide injection into the monolayer subphase. We were very surprised that the Short-peptide was soluble in the polar solvent methanol because it is mainly composed of the long stretch of 21 hydrophobic amino acids (Table 1). However, the charged amino acids at the end of its C-terminus may allow explaining this observation. The comparison of the spectroscopic properties of the Long- and Short-peptides in powder and when solubilized in MeOH or HFIP provides useful information. The spectra of the Long- and Short-peptides in powder are very different (Fig. 3 and Supplementary Figure S3A). The width of the amide I band of the Short-peptide includes a significant amount of aggregated β-sheets (component at 1620 cm^{-1}) in addition to α-helical (component at 1655 cm^{-1}) structures. There is no evidence for the presence of such aggregated species in the Long-peptide powder. Nonetheless, although the Short-peptide includes aggregated components, it was readily soluble in HFIP and more surprisingly in MeOH. In fact, only slight differences can be seen between the spectra of the Long- and Short-peptides in MeOH and in HFIP (Supplementary Figure S3B and C), which allows to conclude that MeOH and HFIP solubilize the Short-peptide as efficiently as the Long-peptide and that they have a very similar secondary structure in these two solvents. As mentioned in Section 3.4, we have previously observed for the C-terminal hydrophobic segment of lecithin retinol acyltransferase (LRAT), that its structure was more ordered in monolayer than in the solvent used to inject it into the subphase [27]. This is also true for the Long- and Short-peptides of RDH11. Indeed, as can be seen in Supplementary Figure S4A and B, the width of the amide I band of the Long- and Short-peptides is thinner after their adsorption in monolayers than in MeOH. It must be stressed that these data are also showing for the first time that the N-terminal segment, which presumably mediates RDH11 membrane anchoring to microsomal RPE membranes, is structured as an α-helix.

4.2. Effect of lipid monolayers on the structure of the Long- and Short-peptides and their preferential binding to phosphoethanolamine

We have previously observed that lipid monolayers improved the order of the α-helical structure of the C-terminal anchoring segment of LRAT [27]. This is however not entirely true for the N-terminal peptide of RDH11. Indeed, as shown in Fig. 5B, the α-helical structure of the Long-peptide becomes significantly disordered upon binding to DOPC, DOPS and, to a lesser extent, to DOPE. However, its binding to DPPE and, in particular to DSPE, leads to little perturbation of the structure of this peptide (Fig. 5C and Supplementary Figure S2D and E). This might be related to the more rigid environment of the solid-condensed state of DPPE and DSPE, compared to the liquid-expanded state of DOPC, DOPS and DOPE, and also to the length of the fatty acyl chains of DSPE, which likely allows stabilizing the Long-peptide. The amide I/amide II (AI/AII) ratio from PM-IRRAS spectra have been shown to allow determining the orientation of α-helical peptides in monolayers on the basis of simulated spectra [47]. An orientation of 50° and 60° has respectively been calculated for AI/AII ratios of 1.5 and 3.2 with respect to the normal of the monolayer. Therefore, the AI/AII ratio of 1.7 observed for the Long-Peptide in the absence and in the presence of DSPE (Supplementary Figure S2E) thus suggests an orientation of this peptide between 50° and 60°. It has been previously shown that the tilt angle of transmembrane α-helical hydrophobic peptides was larger when the bilayer was thinner [48]. In other words, the α-helical peptide accomodates its orientation to minimize the hydrophobic mismatch. Such a phenomenon likely also takes place in monolayer as the size of the α-helical hydrophobic stretch of the Long-peptide (26 Å) slightly extends the thickness of the DSPE monolayer (24 Å [49]). In addition, the position of the charged amino acids of the Long-peptide and, in particular Arg25, might be also involved in the positioning of this peptide in membranes and monolayers. Supplementary Figure S5 is showing a model of the three-dimensional structure of the Long-peptide, which illustrates the distribution of its hydrophobic/hydrophilic residues surface pattern. It can be seen that a single residue is pointing out of the peptide, i.e. the positively charged Arg25. This arginine may allow stabilizing the anchoring of this peptide by electrostatic interactions with the negatively charged phosphate groups of phospholipids, a phenomenon previously designated as snorkeling [50].

Moreover, the Long-peptide is displaying a highly structured α-helix and a preferential interaction towards phosphoethanolamine. The abundance of this phospholipid in both the macular (67.5%) and peripheral (67.4%) regions of the RPE may be related to this preference of the N-terminal anchoring segment of RDH11 [44]. It has been postulated that membrane anchoring of RDH11 is driven by its N-terminal segment [7] whereas no acylation is required in contrast to some other visual proteins such as rhodopsin [51], RPE65 [52] or RDH8 [53]. However, one can not exclude the involvement of other residues or lipid binding motifs of RDH11 in its membrane interaction. Indeed, given that the substrate of RDH11 is highly hydrophobic, other regions of this protein must also be involved to provide a proper membrane embedding and orientation of the active site of this enzyme. Additional measurements are thus under way to characterize the membrane binding of RDH11 as well as the truncated RDH11 (without its N-terminal segment), which will provide additional information and shall allow to draw conclusions on the role of this segment in the activity and function of RDH11, such as performed with other proteins [54–56]. We have for example previously shown that a truncated LRAT, where its N- and C-terminal transmembrane segments have been removed, was nonetheless showing a strong monolayer binding, most likely to allow membrane embedding of its active site [27]. This might also be true for truncated RDH11. Altogether, the present data demonstrate that adding 11 amino acids on the C-terminal side of the Short-peptide to produce the Long-peptide has resulted in an increase of the stability of the hydrophobic core and of its α-helicity and that the properties of this segment are consistent with those of a transmembrane α-helix. The N-terminal segment of RDH11 is thus likely involved in the membrane anchoring of RDH11.

Acknowledgements

The work described in this paper was supported by the Natural Sciences and Engineering Research Council of Canada (NSERC). M. Lhor was awarded scholarships from the Faculty of Medecine (Université Laval) and the Regroupement Stratégique PROTEO. M. Méthot was the recipient of a Graduate Scholarship from the Canadian Institutes of Health Research (CIHR). H. Horchani was awarded a postdoctoral fellowship from NSERC. The Banque d'Yeux Nationale is partly supported by the Réseau de Recherche en Santé de la Vision from the FRQS. The Centre de recherche du CHU de Québec and PROTEO are supported by infrastructure grants from the FRQS and the FRQNT, respectively.

Appendix A. Supplementary data

Supplementary data to this article can be found online at http://dx.doi.org/10.1016/j.bbamem.2014.12.014.

References

[1] B. Lin, J.T. White, C. Ferguson, S. Wang, R. Vessella, R. Bumgarner, L.D. True, L. Hood, P.S. Nelson, Prostate short-chain dehydrogenase reductase 1 (PSDR1): a new member of the short-chain steroid dehydrogenase/reductase family highly expressed in normal and neoplastic prostate epithelium, Cancer Res. 61 (2001) 1611–1618.

[2] N.Y. Kedishvili, O.V. Chumakova, S.V. Chetyrkin, O.V. Belyaeva, E.A. Lapshina, D.W. Lin, M. Matsumura, P.S. Nelson, Evidence that the human gene for prostate short-chain dehydrogenase/reductase (PSDR1) encodes a novel retinal reductase (RalR1), J. Biol. Chem. 277 (2002) 28909–28915.

[3] F. Haeseleer, G.F. Jang, Y. Imanishi, C.A. Driessen, M. Matsumura, P.S. Nelson, K. Palczewski, Dual-substrate specificity short chain retinol dehydrogenases from the vertebrate retina, J. Biol. Chem. 277 (2002) 45537–45546.

[4] T.S. Kim, A. Maeda, T. Maeda, C. Heinlein, N. Kedishvili, K. Palczewski, P.S. Nelson, Delayed dark adaptation in 11-cis-retinol dehydrogenase-deficient mice: a role of RDH11 in visual processes in vivo, J. Biol. Chem. 280 (2005) 8694–8704.

[5] M. Lhor, C. Salesse, Retinol dehydrogenases: membrane-bound enzymes for the visual function, Biochem. Cell Biol. 92 (2014) 510–523.

[6] A. Kasus-Jacobi, J. Ou, Y.K. Bashmakov, J.M. Shelton, J.A. Richardson, J.L. Goldstein, M.S. Brown, Characterization of mouse short-chain aldehyde reductase (SCALD), an enzyme regulated by sterol regulatory element-binding proteins, J. Biol. Chem. 278 (2003) 32380–32389.

[7] O.V. Belyaeva, A.V. Stetsenko, P. Nelson, N.Y. Kedishvili, Properties of short-chain dehydrogenase/reductase RalR1: characterization of purified enzyme, its orientation in the microsomal membrane, and distribution in human tissues and cell lines, Biochemistry 42 (2003) 14838–14845.

[8] G.F. Jang, J.P. Van Hooser, V. Kuksa, J.K. McBee, Y.G. He, J.J. Janssen, C.A. Driessen, K. Palczewski, Characterization of a dehydrogenase activity responsible for oxidation of 11-cis-retinol in the retinal pigment epithelium of mice with a disrupted RDH5 gene, A model for the human hereditary disease fundus albipunctatusJ. Biol. Chem. 276 (2001) 32456–32465.

[9] M. Monne, G. von Heijne, Effects of 'hydrophobic mismatch' on the location of transmembrane helices in the ER membrane, FEBS Lett. 496 (2001) 96–100.

[10] S.S. Krishnakumar, E. London, Effect of sequence hydrophobicity and bilayer width upon the minimum length required for the formation of transmembrane helices in membranes, J. Mol. Biol. 374 (2007) 671–687.

[11] E. London, K. Shahidullah, Transmembrane vs. non-transmembrane hydrophobic helix topography in model and natural membranes, Curr. Opin. Struct. Biol. 19 (2009) 464–472.

[12] A. Senes, M. Gerstein, D.M. Engelman, Statistical analysis of amino acid patterns in transmembrane helices: the GxxxG motif occurs frequently and in association with β-branched residues at neighboring positions, J. Mol. Biol. 296 (2000) 921–936.

[13] Y. Zhang, I-TASSER server for protein 3D structure prediction, BMC Bioinforma. 9 (2008) 40.

[14] M. Lhor, S.C. Bernier, H. Horchani, S. Bussieres, L. Cantin, B. Desbat, C. Salesse, Comparison between the behavior of different hydrophobic peptides allowing membrane anchoring of proteins, Adv. Colloid Interf. Sci. 207 (2014) 223–239.

[15] J.T. Pelton, L.R. McLean, Spectroscopic methods for analysis of protein secondary structure, Anal. Biochem. 277 (2000) 167–176.

[16] S.M. Kelly, T.J. Jess, N.C. Price, How to study proteins by circular dichroism, Biochim. Biophys. Acta Protein Proteomics 1751 (2005) 119–139.

[17] A. Barth, Infrared spectroscopy of proteins, Biochim. Biophys. Acta 1767 (2007) 1073–1101.

[18] P. Calvez, E.r. Demers, E.l. Boisselier, C. Salesse, Analysis of the contribution of saturated and polyunsaturated phospholipid monolayers to the binding of proteins, Langmuir 27 (2011) 1373–1379.

[19] R. Gautier, D. Douguet, B. Antonny, G. Drin, HELIQUEST: a web server to screen sequences with specific alpha-helical properties, Bioinformatics 24 (2008) 2101–2102.

[20] R.C. Keller, New user-friendly approach to obtain an eisenberg plot and its use as a practical tool in protein sequence analysis, Int. J. Mol. Sci. 12 (2011) 5577–5591.

[21] A. Roy, A. Kucukural, Y. Zhang, I-TASSER: a unified platform for automated protein structure and function prediction, Nat. Protoc. 5 (2010) 725–738.

[22] P. Calvez, S. Bussières, D. Éric, C. Salesse, Parameters modulating the maximum insertion pressure of proteins and peptides in lipid monolayers, Biochimie 91 (2009) 718–733.

[23] M.C. Phillips, C.E. Sparks, Properties of apolipoproteins at the air–water interface, Ann. N. Y. Acad. Sci. 348 (1980) 122–137.

[24] R. Verger, F. Pattus, Lipid–protein interactions in monolayers, Chem. Phys. Lipids 30 (1982) 189–227.

[25] D. Blaudez, T. Buffeteau, J.C. Cornut, B. Desbat, N. Escafre, M. Pezolet, J.M. Turlet, Polarization modulation FTIR spectroscopy at the air-water interface, Thin Solid Films 242 (1994) 146–150.

[26] H. Lavoie, B. Desbat, D. Vaknin, C. Salesse, Structure of rhodopsin in monolayers at the air−water interface: a PM-IRRAS and X-Ray reflectivity study, Biochemistry 41 (2002) 13424–13434.

[27] S. Bussieres, L. Cantin, B. Desbat, C. Salesse, Binding of a truncated form of lecithin: retinol acyltransferase and its N- and C-terminal peptides to lipid monolayers, Langmuir 28 (2012) 3516–3523.

[28] H. Bourque, I. Laurin, M. Pézolet, J.M. Klass, R.B. Lennox, G.R. Brown, Investigation of the poly(l-lactide)/poly(d-lactide) stereocomplex at the air–water interface by polarization modulation infrared reflection absorption spectroscopy, Langmuir 17 (2001) 5842–5849.

[29] D. Blaudez, J.-M. Turlet, J. Dufourcq, D. Bard, T. Buffeteau, B. Desbat, Investigations at the air/water interface using polarization modulation IR spectroscopy, J. Chem. Soc. Faraday Trans. 92 (1996) 525–530.

[30] T. Buffeteau, B. Desbat, J.M. Turlet, Polarization modulation FT-IR spectroscopy of surfaces and ultra-thin films: experimental procedure and quantitative analysis, Appl. Spectrosc. 45 (1991) 380–389.

[31] M. Kozak, Comparison of initiation of protein synthesis in procaryotes, eucaryotes, and organelles, Microbiol. Rev. 47 (1983) 1–45.

[32] C. Giglione, A. Boularot, T. Meinnel, Protein N-terminal methionine excision, Cell. Mol. Life Sci. 61 (2004) 1455–1474.

[33] E.J. Dufourc, S. Buchoux, J. Toupe, M.A. Sani, F. Jean-Francois, L. Khemtemourian, A. Grelard, C. Loudet-Courreges, M. Laguerre, J. Elezgaray, B. Desbat, B. Odaert, Membrane interacting peptides: from killers to helpers, Curr. Protein Pept. Sci. 13 (2012) 620–631.

[34] E. London, Lipid bilayer structure, Encycl. Biol. Chem. (2013) 733–735.

[35] R.W. Woody, Circular dichroism, Methods Enzymol. 246 (1995) 34–71.

[36] S.-W. Ha, T. Asakura, R. Kishore, Distinctive influence of two hexafluoro solvents on the structural stabilization of *Bombyx mori* Silk fibroin protein and its derived peptides: 13C NMR and CD studies, Biomacromolecules 7 (2005) 18–23.

[37] S.K. Haq, R.H. Khan, Effect of detergents and hexafluoroisopropanol on the conformation of a non-helical and a helical plant protease inhibitor, Int. J. Biol. Macromol. 36 (2005) 47–53.

[38] P. Pancoska, E. Bitto, V. Janota, M. Urbanova, V.P. Gupta, T.A. Keiderling, Comparison of and limits of accuracy for statistical analyses of vibrational and electronic circular dichroism spectra in terms of correlations to and predictions of protein secondary structure, Protein Sci. 4 (1995) 1384–1401.

[39] E. Goormaghtigh, V. Raussens, J.-M. Ruysschaert, Attenuated total reflection infrared spectroscopy of proteins and lipids in biological membranes, Biochim. Biophys. Acta 1422 (1999) 105–185.

[40] E. Goormaghtigh, V. Cabiaux, J.M. Ruysschaert, Determination of soluble and membrane protein structure by Fourier transform infrared spectroscopy. I. Assignments and model compounds, Subcell. Biochem. 23 (1994) 329–362.

[41] N.A. Nevskaya, Y.N. Chirgadze, Infrared spectra and resonance interactions of amide-I and II vibration of alpha-helix, Biopolymers 15 (1976) 637–648.

[42] A. Blume, A. Kerth, Peptide and protein binding to lipid monolayers studied by FT-IRRA spectroscopy, Biochim. Biophys. Acta 1828 (2013) 2294–2305.

[43] G. Brezesinski, H. Mohwald, Langmuir monolayers to study interactions at model membrane surfaces, Adv. Colloid Interf. Sci. 100–102 (2003) 563–584.

[44] H.G. Gulcan, R.A. Alvarez, M.B. Maude, R.E. Anderson, Lipids of human retina, retinal pigment epithelium, and Bruch's membrane/choroid: comparison of macular and peripheral regions, Invest. Ophthalmol. Vis. Sci. 34 (1993) 3187–3193.

[45] D. Marsh, Lateral pressure in membranes, Biochim. Biophys. Acta 1286 (1996) 183–223.

[46] G.D. Henry, B.D. Sykes, Methods to study membrane protein structure in solution, Methods Enzymol. 239 (1994) 515–535.

[47] I. Cornut, B. Desbat, J.M. Turlet, J. Dufourcq, In situ study by polarization modulated Fourier transform infrared spectroscopy of the structure and orientation of lipids and amphipathic peptides at the air-water interface, Biophys. J. 70 (1996) 305–312.

[48] S.H. Park, S.J. Opella, Tilt angle of a trans-membrane helix is determined by hydrophobic mismatch, J. Mol. Biol. 350 (2005) 310–318.

[49] D. Ducharme, J.J. Max, C. Salesse, R.M. Leblanc, Ellipsometric study of the physical states of phosphatidylcholines at the air-water interface, J. Phys. Chem. 94 (1990) 1925–1932.

[50] J.A. Killian, G. von Heijne, How proteins adapt to a membrane–water interface, Trends Biochem. Sci. 25 (2000) 429–434.

[51] A. Ovchinnikov Yu, N.G. Abdulaev, A.S. Bogachuk, Two adjacent cysteine residues in the C-terminal cytoplasmic fragment of bovine rhodopsin are palmitylated, FEBS Lett. 230 (1988) 1–5.

[52] L. Xue, D.R. Gollapalli, P. Maiti, W.J. Jahng, R.R. Rando, A palmitoylation switch mechanism in the regulation of the visual cycle, Cell 117 (2004) 761–771.

[53] W. Luo, N. Marsh-Armstrong, A. Rattner, J. Nathans, An outer segment localization signal at the C terminus of the photoreceptor-specific retinol dehydrogenase, J. Neurosci. 24 (2004) 2623–2632.

[54] J.F. Chich, C. Chapuis, C. Henry, J. Vidic, H. Rezaei, S. Noinville, Vesicle permeabilization by purified soluble oligomers of prion protein: a comparative study of the interaction of oligomers and monomers with lipid membranes, J. Mol. Biol. 397 (2010) 1017–1030.

[55] M. van Geest, J.S. Lolkema, Membrane topology and insertion of membrane proteins: search for topogenic signals, Microbiol. Mol. Biol. Rev. 64 (2000) 13–33.

[56] D. Stoddart, M. Ayub, L. Hofler, P. Raychaudhuri, J.W. Klingelhoefer, G. Maglia, A. Heron, H. Bayley, Functional truncated membrane pores, Proc. Natl. Acad. Sci. U. S. A. 111 (2014) 2425–2430.